

High magma decompression rates at the peak of a violent caldera-forming eruption (Lower Pumice 1 eruption, Santorini, Greece)

J. M. Simmons¹ · R. J. Carey² · R.A.F. Cas^{1,2} · T. H. Druitt³

Received: 12 February 2017 / Accepted: 9 April 2017 / Published online: 8 May 2017
© Springer-Verlag Berlin Heidelberg 2017

Abstract We use the deposit sequence resulting from the first catastrophic caldera collapse event recorded at Santorini (associated with 184 ka Lower Pumice 1 eruption), to study the shallow conduit dynamics at the peak of caldera collapse. The main phase of the Lower Pumice 1 eruption commenced with the development of a sustained buoyant eruption column, producing a clast-supported framework of rhyodacitic white pumice (LP1-A). The clasts have densities of 310–740 kg m⁻³, large coalesced vesicles that define unimodal size distributions and moderate to high vesicle number densities (1.2×10^9 – 1.7×10^9 cm⁻³). Eruption column collapse, possibly associated with incipient caldera collapse, resulted in the development of pyroclastic flows (LP1-B). The resulting ignimbrite is characterised by rhyodacitic white pumice with a narrow density range (250–620 kg m⁻³) and moderate to high vesicle number densities (1.3×10^9 – 2.1×10^9 cm⁻³), comparable to clasts from LP1-A. An absence of deep, basement-derived lithic clast assemblages, together with the occurrence of large vesicles and relatively high vesicle number densities

in pumice from the fallout and pyroclastic flow phases, suggests shallow fragmentation depths, a prolonged period of bubble nucleation and growth, and moderate rates of decompression prior to fragmentation (7–11 MPa s⁻¹). Evacuation of magma during the pyroclastic flow phase led to underpressurisation of the magma reservoir, the propagation of faults (associated with the main phase of caldera collapse) and the formation of 20 m thick lithic lag breccias (LP1-C). Rhyodacitic pumices from the base of the proximal lithic lag breccias show a broader range of density (330–990 kg m⁻³), higher vesicle number densities (4.5×10^9 – 1.1×10^{10} cm⁻³) and higher calculated magma decompression rates of 15–28 MPa s⁻¹ than pyroclasts from the pre-collapse eruptive phases. In addition, the abundance of lithic clasts, including deeper, basement-derived lithic assemblages, records the opening of new vents and a deepening of the fragmentation surface. These data support numerical simulations which predict rapid increases in magma decompression and mass discharge rates at the onset of caldera collapse.

Editorial responsibility: V. Acocella

Electronic supplementary material The online version of this article (doi:10.1007/s00445-017-1120-1) contains supplementary material, which is available to authorized users.

✉ J. M. Simmons
jack.simmons@monash.edu

¹ School of Earth, Atmosphere and Environment (EAE), Monash University, Clayton, VIC, Australia

² School of Earth Sciences/CODES, University of Tasmania, Hobart, TAS, Australia

³ Laboratoire Magmas et Volcans, Université Clermont Auvergne CNRS, IRD, OPGC, 6 Avenue Blaise Pascal, 63178 Clermont-Ferrand, France

Keywords Vesicle textures · Pumice · Magma decompression · Caldera collapse · Lower Pumice 1 · Santorini

Introduction

The timing and style of caldera collapse strongly controls the pressure conditions in the magma reservoir and conduits, which in turn modulate the eruption dynamics and temporal evolution of explosive eruptions (Gudmundsson 1998; Klug et al. 2002; Folch and Martí 2009; Andrews and Gardner 2010; Vinkler et al. 2012). Many calderas form due to magma withdrawal and underpressurisation of the magma reservoir, leading to the opening of marginal fractures, subsidence along outward-dipping and inward-dipping faults and breakup of the

roof block (Gudmundsson 1998; Acocella et al. 2000), producing ignimbrites and lithic lag breccias (Druitt 1985; Walker 1985; Druitt and Bacon 1986; Allen and Cas 1998). Juvenile magmatic pyroclasts erupted during these events record reservoir and conduit processes (e.g. Klug et al. 2002; Houghton et al. 2010; Alfano et al. 2012; Vinkler et al. 2012), whereas lithic clast assemblages can record changes in fragmentation depth in the conduit (e.g. Suzuki-Kamata et al. 1993; Rosi et al. 1996; Pittari et al. 2008; Vinkler et al. 2012; Druitt 2014). The vesicularity characteristics of pumice, in particular, can help quantify magma decompression rate, and when studied in their stratigraphic context, changes in decompression rate with time (e.g. Toramaru 2006; Shea et al. 2011; Vinkler et al. 2012). Together, these data provide a record of the temporal evolution of physical conditions in the reservoir, conduit and vent. Here, we describe the deposits of a pyroclastic fall and pyroclastic flow, as well as lithic lag breccias produced at the climax of 184 ka rhyodacitic Lower Pumice 1 eruption of Santorini. In particular, we quantify the microtextures of juvenile silicic pumice pyroclasts from each phase and calculate magma decompression rates. We present geological arguments that the climactic phase of the LP1 eruption accompanied caldera collapse, and we use our results to

test numerical simulations that predict steep pressure drops in the magma reservoir and conduit at the onset of caldera collapse, followed by re-pressurisation of the magma reservoir as the roof block subsides (Folch and Marti 2009).

Santorini caldera: its setting, evolution and stratigraphy

Santorini is a continental arc caldera volcano, situated within the rapidly extending Aegean microplate (Fig. 1a; Jackson 1994). The Aegean crust, on which Santorini is built, consists of Proterozoic and Mesozoic assemblages (sedimentary, igneous and metamorphic) that were metamorphosed to blueschist and greenschist facies during the Eocene and Miocene, respectively, a consequence of the Alpine orogeny (Andriessen et al. 1979; Papanikolaou 1987; Schliestedt et al. 1987). Greenschist facies assemblages, including limestones, metapelites and schists, crop out at isolated exposures in the caldera wall and at other extra-caldera localities on Thera, the largest of five islands defining Santorini (Nicholls 1971; Druitt et al. 1999). These islands record over 360 kyr of explosive activity, including 12 major explosive eruptions

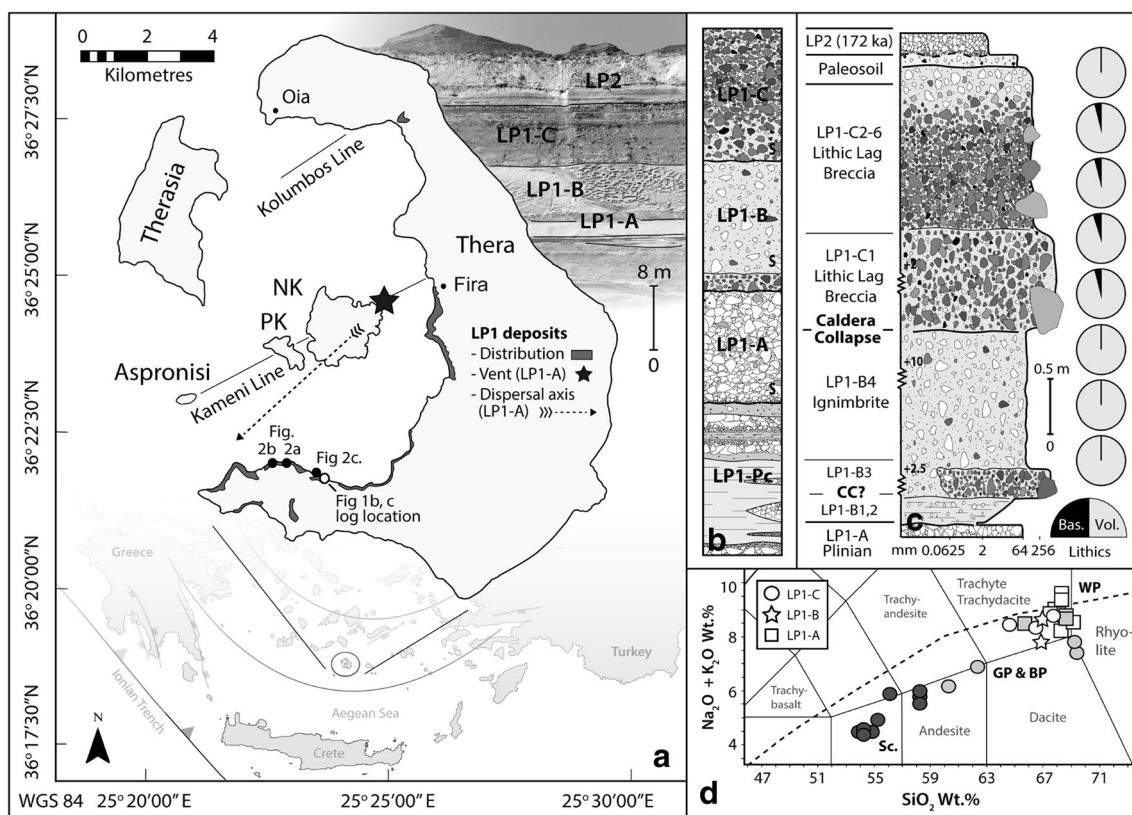


Fig. 1 **a** Tectonic setting of Santorini Volcano within the broader framework of the Aegean microplate. *NK* Nea Kameni, *PK* Palea Kameni (after Druitt et al. 1999). **b** Stratigraphy of the LP1 eruption sequence. *S* sampled stratigraphic levels. **c** Detailed stratigraphy of the LP1-B and -C eruptive phases. Pie charts illustrate the stratigraphic

transition in lithic components from solely upper crustal volcanic lithic assemblages (-B) to increasingly diverse basement and volcanic derived lithic assemblages (-C). *Bas.* basement lithics, *Vol.* volcanic lithics. **d** Compositions of white (*WP*), grey (*GP*) and banded (*BP*) pumice, and scoria (*Sc*) from the LP1 deposits (Druitt et al. 1999; Simmons et al. 2016)

(VEI 5–7) and five major caldera-forming events, associated with the 184 ka Lower Pumice 1, 172 ka Lower Pumice 2, 80 ka Upper Scoriae 1, 21 ka Cape Riva and 3.6 ka Minoan eruptions, respectively (Druitt and Francaviglia 1992; Druitt et al. 1999; Keller et al. 2000; Vespa et al. 2006; Gertisser et al. 2009; Simmons et al. 2016).

The 184 ka rhyodacitic Lower Pumice 1 eruption

The Lower Pumice 1 eruption, the focus of this article, was one of the earliest rhyodacitic explosive eruptions at Santorini. It had a precursory phase of relatively weak eruptions (<4 m thick deposits; LP1-Pc), followed by a magmatic Plinian phase (<30 m thick deposits; Figs. 1b, 2a; Druitt et al. 1999; Simmons et al. 2016). The Plinian phase transitioned from an initially buoyant to collapsing eruption column, producing a rhyodacitic pumice fall (<6 m thick; LP1-A) and pyroclastic flow deposit (<13 m thick; LP1-B), with minor, fresh, upper crustal, accessory volcanic lithic clasts (<5%; flow-banded dacite, aphanitic basaltic andesites, phyrlic basalts, scoriaceous basalts, obsidian and hornblende-bearing tuff fragments; Figs. 1c, 2a; Simmons et al. 2016). The eruption concluded with the discharge of lithic-rich pyroclastic flows and ballistics (ejected at around 200–300 m s⁻¹), associated with a major vent excavation event, and the deposition of a <20 m thick sequence of lithic-rich lag breccias (LP1-C; Fig. 2b–d). The breccias are variably matrix to clast-supported, dominated by hydrothermally altered and fresh accessory volcanic lithic clasts (~80–90%), subordinate

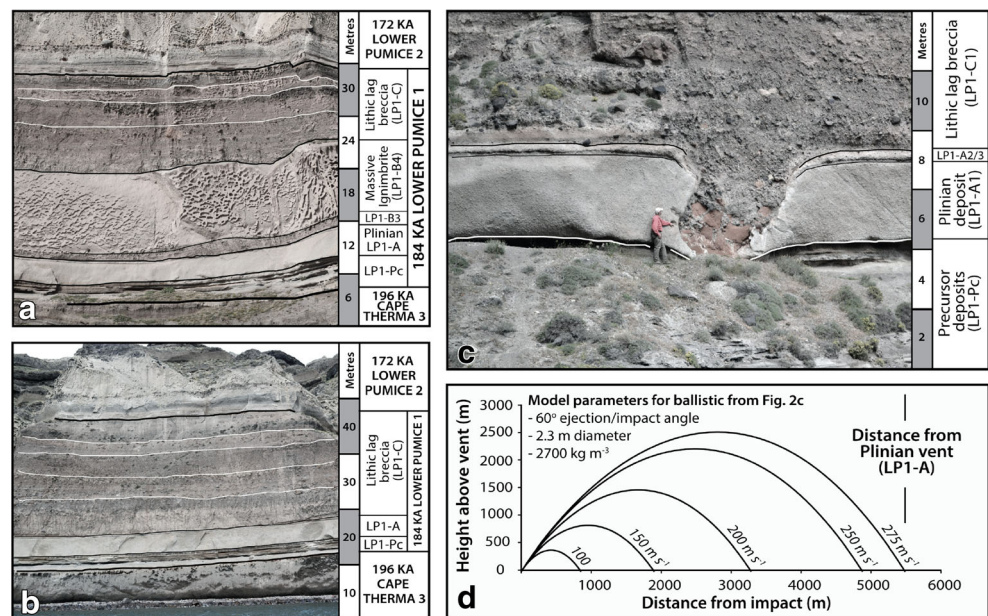
rhyodacitic white pumice (at the base of LP1-C) and basaltic-andesitic scoria (towards the top of LP1-C; Fig. 1d; Druitt et al. 1999; Simmons et al. 2016). In addition to containing shallow volcanic lithics, similar to those present in the underlying ignimbrite, the lag breccias also contain basement-derived lithic blocks (metapelites, schists, limestone, marble, metasandstones and granitoids; <5%; Fig. 1c; Simmons et al. 2016).

Methods

Sampling: juvenile or recycled pumice pyroclasts?

As the basis for this research, 50–100 juvenile rhyodacitic pumice pyroclasts (between 16 and 24 mm in diameter) were sampled from the base of the LP1 fallout (-A1), ignimbrite (-B4) and lithic-rich lag breccia (-C1). The clasts from LP1-A1 were deposited by fallout from a buoyant eruption column. This contrasts to the ignimbrites and lithic lags breccias of LP1-B and LP1-C, respectively, which were deposited from pyroclastic (ground-hugging) density currents. It is therefore conceivable that pyroclasts deposited during the early history of Santorini (including the underlying precursory and Plinian fall deposits of the LP1 eruption) were incorporated into the pyroclastic flow, contaminating what would otherwise be a representative sample population. We discount this possibility for several reasons. First, pyroclasts from ignimbrite and lithic lag breccia are characteristically angular, suggesting minor to no reworking. Second, the densities of pumice from the lithic lag breccia (LP1-C1) are significantly more variable than clasts from the underlying fall (LP1-A1) and flow (LP1-B4) deposits,

Fig. 2 a and b Field photos of the LP1 deposits within the caldera wall sequence. Note the thickness of the lithic lag breccias (LP1-C) and the absence of the LP1-B ignimbrite in Fig. 2b. c Ballistic impact sag structure with a jigsaw-fit, hydrothermally altered, lithic bomb that intrudes into the underlying fall deposit of LP1-A. See Fig. 1a for photo locations. d Modelled trajectories for the LP1-C ballistic bomb from Fig. 2c (assuming equivalent discharge and impact heights), determined using the program ‘Eject!’ (Mastin 2001)



which have much smaller density modes. We also discount the possibility that pumice from the precursor deposits were remobilised (despite comparable density distributions to LP1-C1), because the precursor clasts have higher crystal contents and less evolved compositions (low to moderate crystal contents ~15%; dacitic) than pumice from the Plinian deposit sequence (crystal-poor <3%; rhyodacitic; Simmons et al. 2016). We therefore interpret the majority of pumice in the ignimbrite and lithic lag breccia as newly erupted.

Density and vesicularity analysis

The densities (kg m^{-3}) and total vesicularities ($V_{\text{T}} = \text{vol } \%$) of juvenile rhyodacitic pyroclasts (between 16 and 24 mm) were determined using the method of Silva (2008) at the Université Clermont Auvergne's Laboratoire de Magmas, in Clermont-Ferrand, France (see supplementary material). Representative clasts from the low, modal and high density populations were then sectioned and imaged using a JEOL 7001F SEM. Pumice vesicle textures were imaged at four different magnifications (section scan, $\times 25$, $\times 100$ and $\times 500$ —15 images total) to capture the spectrum of vesicle sizes, as per the method of Shea et al. (2010). The nested images were then imported into Adobe Photoshop and converted to binary images (white—glass, black—vesicle). This process involved minor vesicle wall reconstruction. The images were then analysed in FOAMS, a Matlab program, which uses the stereological conversion technique of Sahagian and Proussevitch (1998) to characterise vesicle size distributions and quantify vesicle number density (Shea et al. 2010). As in Shea et al. (2011), vesicle number densities were only determined for vesicle sizes between 1 and 10 μm (N_{V}). Such vesicle sizes are considered to represent the final nucleation event prior to magma fragmentation and therefore final decompression rates (Shea et al. 2011). This also has the effect of excluding coalesced vesicles which form at vesicularities >75 vol % (Rotella et al. 2014). N_{V} was then corrected for vesicularity and melt/glass fraction ($N_{\text{VF}} = N_{\text{V}}/\text{glass fraction}$), to enable the accurate determination of true vesicle number density (e.g. Klug et al. 2002; Adams et al. 2006; Houghton et al. 2010; Shea et al. 2011; Vinkler et al. 2012).

Results

Juvenile clast density and vesicularity

Rhyodacitic pumices from the fall deposit (LP1-A1), ignimbrite (LP1-B4) and lithic lag breccia (LP1-C1) differ markedly in terms of density. Those from the fall deposit define a unimodal, low density distribution (310–740 kg m^{-3}), with vesicularities of 71–88 vol % and modal density values of 500–550 kg m^{-3} (Fig. 3a bottom). The clasts have moderate

to large and round vesicles (mode of 79–198 μm), with thin, wrinkled and ruptured vesicle walls indicative of bubble expansion and coalescence (Fig. 3b, c bottom). N_{VF} values range from 1.2×10^9 to $1.7 \times 10^9 \text{ cm}^{-3}$. Pumice clasts from the ignimbrite have a narrower density distribution (250–620 kg m^{-3}), lower modes (350–400 kg m^{-3}) and higher vesicularities (76–90 vol %), characterised by broadly unimodal vesicle size distributions with modes around 50 μm (Fig. 3a, b centre). The vesicles have round to oblique shapes and very thin glass walls (1–10 μm). Vesicles >370 μm in diameter are randomly dispersed within the pumices and are variably bound by regions of elongated and stretched vesicles (Fig. 3c centre). These clasts have a narrow range of N_{VF} from 1.3×10^9 to $2.1 \times 10^9 \text{ cm}^{-3}$, similar to pumice from LP1-A1. In stark contrast, pumices from the lithic breccia have a significantly broader density distribution (330–990 kg m^{-3}) and vesicularities shifted towards lower values (61–87 vol %), with additional modes at higher densities of 600–650 kg m^{-3} and 750–800 kg m^{-3} . In fact, there is very little overlap in terms of pumice clast density between the ignimbrite and lag breccia, and the densities of pumice from the dominant modes vary by up to 200 kg m^{-3} (Fig. 3a top). The vesicles in pumice from LP1-C1 are also smaller (modes between 20 and 50 μm), more variable in shape (round to elongate), have thin to very thick glass walls and often preserve domains of round microvesicles (1–20 μm ; Fig. 3b, c top). N_{VF} are subsequently higher (half an order of magnitude) in pumice from the lithic lag breccia compared to pumice from the fallout and ignimbrite-forming phases, ranging from 4.5×10^9 to $1.1 \times 10^{10} \text{ cm}^{-3}$ (Table 1).

Magma decompression rate

Magma decompression rates can be estimated using nucleation theory when vesicle number densities are measured and magma properties are known (Toramaru 2006; Shea et al. 2011), as follows:

$$\text{Decompression rate } \left(\frac{dp}{dt} \right) = a \times D \times \sigma^2 \times P_{\text{W}}^{-1/3} \times T^{-1/2} \times N_{\text{VF}}^{2/3}, \quad (1)$$

where a is a constant ($=1 \times 10^{15}$), D is the diffusivity of water in a silicate magma ($\text{m}^2 \text{ s}^{-1}$), σ is surface tension (N m^{-1}), P_{W} is saturation pressure (MPa), T is temperature (in K) and N_{VF} is the number density of vesicles of 1–10 μm . Since only a fraction of the initial water content contributed to bubble nucleation and growth during late-stage magma ascent, initial water contents were corrected based on the porosity of vesicles >10 μm (i.e. bubbles which formed as a consequence of degassing prior to late-stage

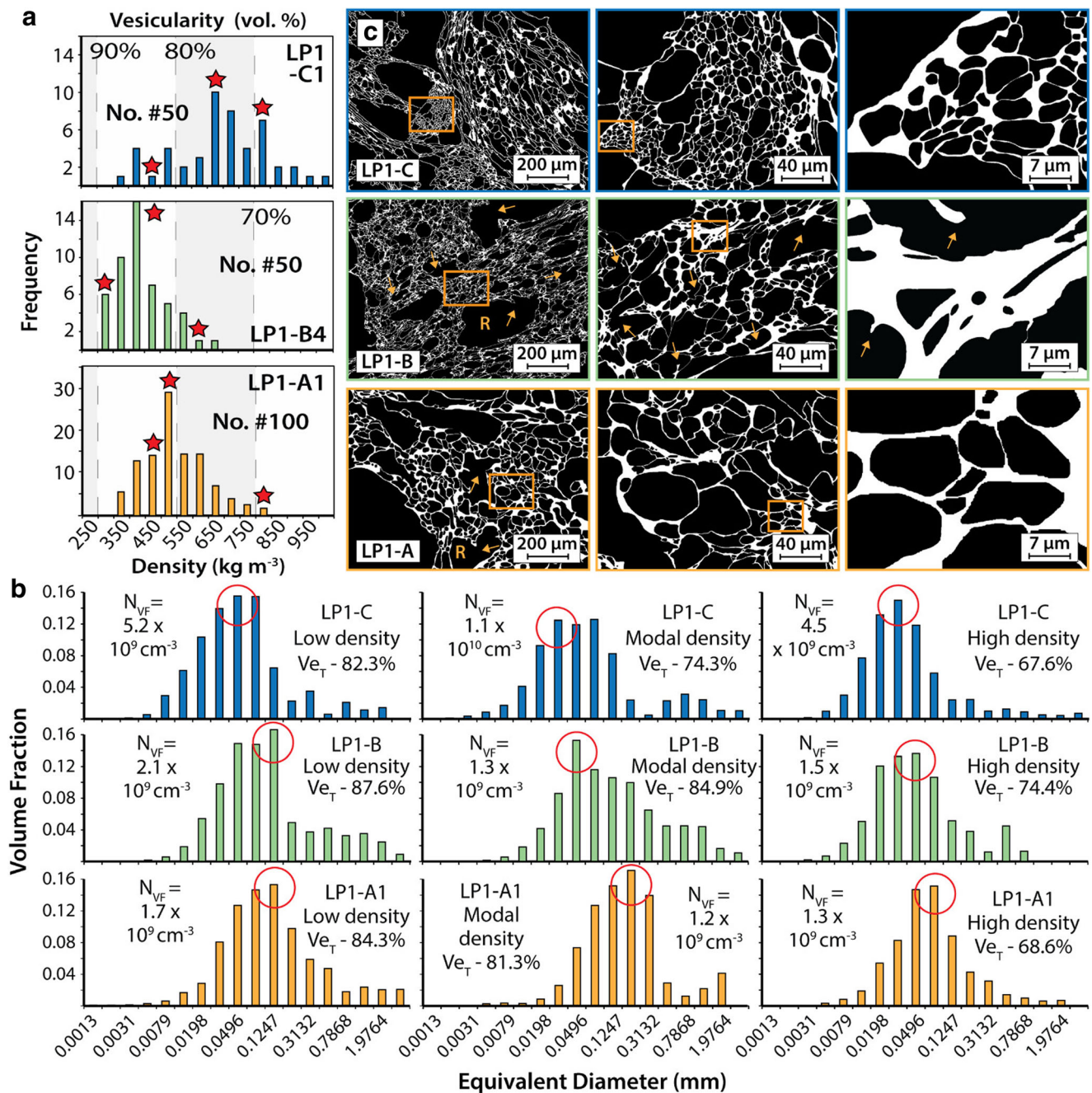


Fig. 3 **a** Histograms illustrating the contrasting density distributions for rhyodacitic pumices from the fallout deposit (-A; orange), ignimbrite (-B; green) and lithic lag breccia (-C; blue). Bin size 50 kg m⁻³. Stars denote designated density classes (low, modal and high densities) from which clasts were selected for 2D image analysis (data from Simmons et al. 2016). **b** Vesicle volume distributions for low, modal and high density pyroclasts from each eruptive unit. **c** Characteristic vesicle textures for

pyroclasts from the fallout deposit, ignimbrite and lithic lag breccia. From the left to the right, each image denotes low (×100), medium (×500) and high (×3000) magnifications, respectively. Juvenile pyroclasts from the lithic lag breccia are distinguished from the fall deposit and ignimbrite by having larger vesicle number densities and a significant fraction of small, spherical vesicles. No clast preserves evidence for magma outgassing and bubble collapse. *R* ruptured vesicle/bubble walls

magma ascent), as per the equilibrium models of Gardner et al. (1999) and Shea et al. (2011):

$$X_F(C_W) = X_I \cdot \frac{\varnothing}{\frac{P}{Z} \overline{V}_W (1-\varnothing)} \tag{2}$$

where X_F/C_W is the final water content, X_I is the initial water content (6.3 wt %; Cadoux et al. 2014), \varnothing is the porosity of vesicles >10 μm, P is the magma density (2300 kg m⁻³), Z is the molecular weight of water (18 g mol⁻¹) and \overline{V}_W is the molar volume of water in the vapour phase. X_F/C_W replaced X_I in all subsequent

Table 1 Summary data for analysed pumice pyroclasts from the fall deposit (LP1-A1), ignimbrite (LP1-B4) and lithic lag breccia (LP1-C1)

| Unit | SiO ₂ content | Den. class | Ve _T % | Vesicle size mode (μm) | Vol. frac % < 10 μm | N _{VF} 1–10 μm (cm ⁻³) | dp/dt (MPa s ⁻¹) |
|--------|--------------------------|------------|-------------------|------------------------|---------------------|---|------------------------------|
| LP1-C1 | 68.1% | Low | 82.3 | 50 | 9.77 | 5.2 × 10 ⁹ | 17.5 |
| | | Mode | 74.3 | 31 | 7.24 | 1.1 × 10 ¹⁰ | 28.4 |
| | | High | 67.6 | 31 | 11.97 | 4.5 × 10 ⁹ | 15.3 |
| LP1-B4 | 67.1% | Low | 87.6 | 125 | 2.56 | 2.1 × 10 ⁹ | 10.5 |
| | | Mode | 84.9 | 50 | 2.47 | 1.3 × 10 ⁹ | 7.4 |
| | | High | 74.4 | 50 | 5.07 | 1.5 × 10 ⁹ | 7.4 |
| LP1-A1 | 68.5% | Low | 84.3 | 125 | 2.44 | 1.7 × 10 ⁹ | 8.9 |
| | | Mode | 81.3 | 187 | 1.00 | 1.2 × 10 ⁹ | 6.8 |
| | | High | 68.6 | 75 | 3.13 | 1.3 × 10 ⁹ | 6.9 |

The composition of clasts analysed from each unit is representative of clasts from those stratigraphic levels (Simmons et al. 2016)

Ve_T total vesicularity, Vol. frac % < 10 μm sample volume occupied by vesicles < 10 μm, N_{VF} vesicularity/melt-corrected number density of vesicles of 1–10 μm, dp/dt magma decompression rate calculated as per the method of Toramaru (2006)

calculations. Diffusivity was first determined using the method of Zhang and Behrens (2000), where melt

temperature (*T*), nucleation pressure (*P*) and final water contents (*X_F/C_W*) are known:

D (Zhang and Behrens, 2000)

$$= X \cdot \exp(m) \cdot \left\{ 1 + \exp \left[56 + m + X \cdot \left(-34 + \frac{44620}{T} + \frac{57.3(P \times 10^{-6})}{T} \right) - \sqrt{X} \cdot \left(0.091 + \frac{4.77 \times 10^6}{T^2} \right) \right] \right\}, \quad (3)$$

where

$$X \text{ (mole fraction of water)} = 0.0167C_W \quad (4)$$

$$m = -20.79 - \frac{5030}{T} - \frac{1.4(P \times 10^6)}{T} \quad (5)$$

$$P = 20000 \times 10^6 \times X^2 \text{ and}$$

$$T \text{ is the temperature of the melt} \quad (6)$$

(1142° K for the LP1 eruption; Cadoux et al. 2014)

Diffusivity was then calculated using the method of Behrens et al. (2004), where temperature, pressure and silica

content (*C_S*) are known, assuming 1 wt % water.

D (Behrens et al. 2004)

$$= 10^{(-0.757 - 0.0868C_S) + \left(\frac{-14785 + 131.7C_S}{T} \right) + \left(\frac{(3.079 - 0.049C_S)(P \times 10^6)}{T} \right)} \quad (7)$$

As in Toramaru (2006), the results from these calculations were combined, resulting in a rate of diffusion that considers melt properties (silica content, water content, temperature etc.).

$$D = D \text{ (Behrens et al. 2004)} \cdot \frac{D \text{ (Zhang and Behrens 2000—Assuming final water content)}}{D \text{ (Zhang and Behrens 2000—Assuming 1 wt. \%water)}} \quad (8)$$

Instead of using the method of Bagdassarov et al. (2000) to calculate surface tension, as in Toramaru (2006), we use an effective surface tension of 0.075 N m⁻¹, which is typical for homogeneous nucleation in dacitic to rhyodacitic melts (Gardner et al. 2013). The method of Bagdassarov et al. (2000) often results in the determination of infeasibly high surface tensions and calculated magma decompression rates.

Based on magma temperatures of 1142 °K (869 °C), calculated magma decompression rates of 7–9 MPa s⁻¹ and 7–11 MPa s⁻¹ were determined for the fall and ignimbrite-forming phases, respectively. This contrasts with pumice from the lag breccias, which have calculated magma decompression rates two to three times higher of 15–28 MPa s⁻¹.

Interpretation and discussion

Evidence of caldera collapse?

Although there is no direct evidence for a LP1 caldera, a consequence of more recent caldera collapse events which have obliterated and overprinted the existing eruption centre, its former presence is supported by two observations. First, the subsequent 172 ka Lower Pumice 2 eruption was in part strongly phreatomagmatic, suggesting the existence of a flooded caldera that was formed during the LP1 eruption (Druitt et al. 1999). Second, lithic breccias, comparable in thickness and lithology to the lag breccias of LP1-C, were produced during subsequent caldera-forming events on Santorini (c.f. lag breccias of the Lower Pumice 2, Cape Riva and Minoan eruptions; Druitt et al. 1999). Such deposits are also a common product of ignimbrite eruptions elsewhere, erupted and deposited contemporaneously at the peak of caldera collapse (Table 2; Druitt 1985; Walker 1985; Druitt and Bacon 1986; Allen and Cas 1998; Pittari et al. 2008; Vinkler et al. 2012).

Magma decompression prior to the caldera-forming phase

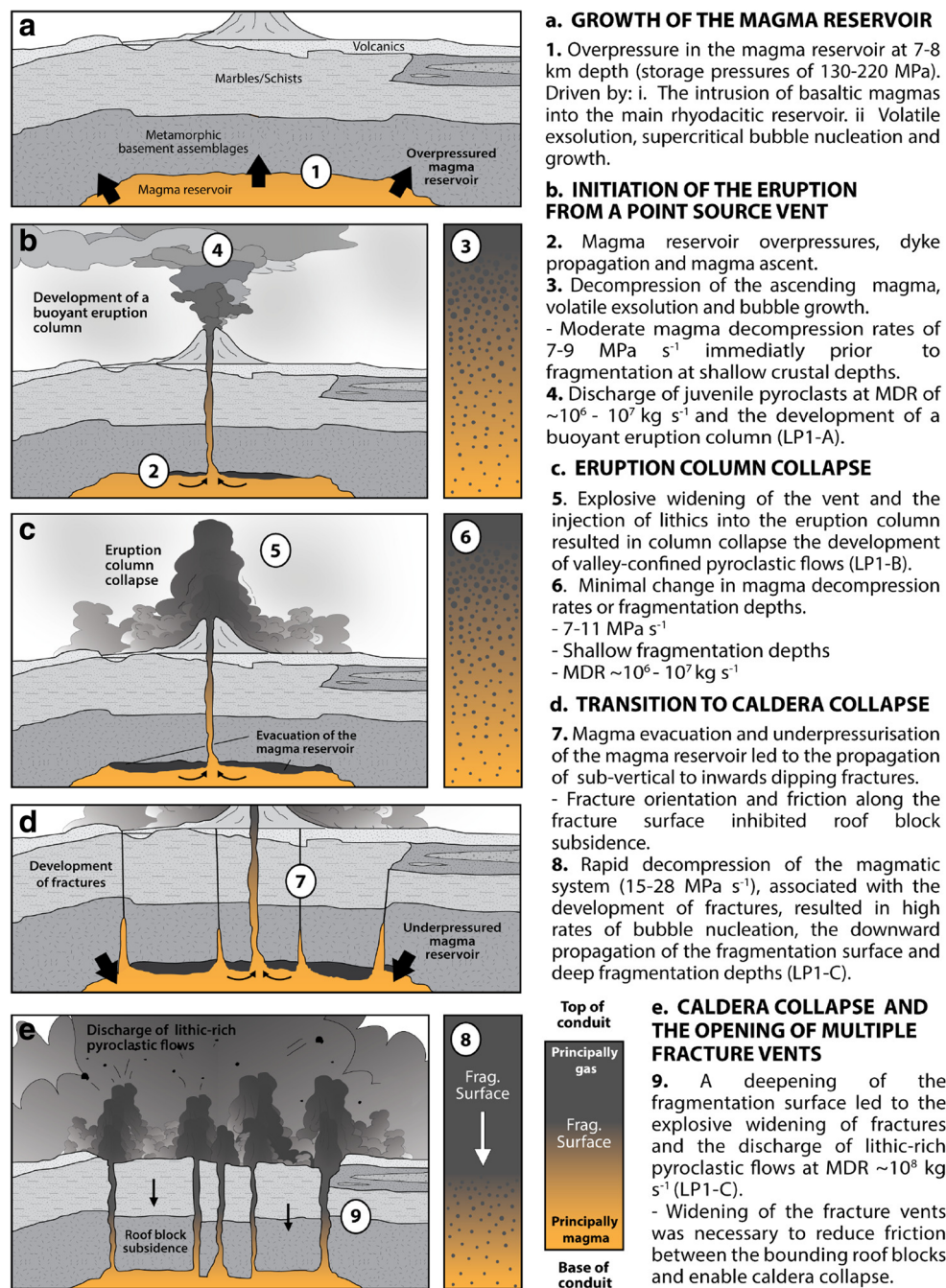
The restricted range of pyroclast textures, vesicularities and N_{VF} in pumice from LP1-A and -B, in addition to the

predominance of expanded and coalesced vesicle with large modes, indicates an extended period of degassing, bubble nucleation and growth prior to the fragmentation of a relatively homogeneous magma foam. Interestingly, such textural features are typical of many pyroclasts from ignimbrites that have experienced post-fragmentation expansion (e.g. unit 6–1.8 ka Taupo Ignimbrite; Houghton et al. 2010). However, we discount the influence of post-fragmentation expansion due to the absence of core to rim vesicle textures in the analysed clasts that would otherwise be reflected by fine vesicle rinds and coarsely vesicular interiors (Houghton et al. 2010). Crystallisation experiments, based on the composition of the analysed pyroclasts (rhyodacite), indicate that at confining pressure of 220 MPa and magma temperatures of 1142 °K, volatile saturation occurs at 7 wt % water (Cadoux et al. 2014). Based on maximum measured water contents of 6.3 wt %, the LP1-A and -B magmas were likely volatile-saturated (mainly H₂O) at storage pressures of 130–220 MPa, exsolving homogeneously prior to late-stage magma ascent (Cadoux et al. 2014). We discount the role of heterogeneous nucleation due to the relatively high vesicle number densities in pumice, the lack of microlites and the occurrence of relatively few phenocrysts (e.g. Mourtada-Bonnefoi and Laporte 2002). Magmatic overpressures, a consequence of volatile exsolution and the late-stage intrusion of more

Table 2 Examples of Plinian eruptions with caldera collapse associated breccias

| Country | Volcanic centre | Eruption | Reference |
|------------------------|--|-------------------------------|--|
| Azores (Portugal) | São Miguel | 4.6 ka Fogo A | Pensa et al. (2015) |
| Canary Islands (Spain) | Tenerife | >170 ka Abrigo Ignimbrite | Pittari et al. (2008) |
| Greece | Kos Santorini | 160 ka Kos Plateau Tuff | Allen and Cas (1998) |
| | | 3.6 ka Minoan | Druitt et al. (1999), Druitt (2014) |
| | | 21 ka Cape Riva | Druitt (1985) |
| | | ~80 ka Upper Scoriae 1 | Druitt et al. (1999) |
| | | 172 ka Lower Pumice 2 | Druitt et al. (1999) |
| Indonesia | Batur Volcanic Field (Bali) | 20.2 ka Gunungkawi Ignimbrite | Reubi and Nicholls (2004) |
| | | 29.3 ka Ubud Ignimbrite | |
| Italy | Phlegraean Fields Ischia Island Vico Caldera Latera Volcanic Complex (Vulsini Volcano) | 36 ka Campanian Ignimbrite | Rosi et al. (1996) |
| | | 55 ka Monte Epomeo Green Tuff | Brown et al. (2008) |
| | | 151 ka Sutri eruption | Bear et al. (2009) |
| | | 170 ka Onano eruption | Palladino and Simei (2005) |
| Japan | Kutcharo Volcano | 120 ka Kutcharo IV eruption | Hasegawa et al. (2016) |
| New Zealand | Taupo Caldera (Taupo Volcanic Zone) Rotorua Caldera (Taupo Volcanic Zone) Reporoa Caldera (Taupo Volcanic Zone) Haroharo Caldera (Taupo Volcanic Zone) | 26.5 ka Oruanui eruption | Wilson (2001) |
| | | 220–230 ka Mamaku Ignimbrite | Milner et al. (2003) |
| | | 240 ka Kaingaroa Ignimbrite | Nairn et al. (1994) |
| | | 280 ka Matahina Ignimbrite | Bailey (1994) |
| USA | Mt. Mazama | 7.7 ka Crater Lake eruption | Druitt and Bacon (1986) Suzuki-Kamata et al. (1993) |

Fig. 4 Simplified diagram illustrating the interpreted transition to caldera collapse during the Lower Pumice 1 eruption



primitive magmas into the magma reservoir (i.e. compositional zonation of LP1-C; Fig. 1d), resulted in dyke propagation and magma ascent (Fig. 4a). The relatively high number densities of small round vesicles in pumice from the fallout and pyroclastic flow phases (1.2×10^9 – 2.1×10^9 cm⁻³), together with the absence of basement-derived lithic assemblages in the deposits, suggest accelerated rates of magma decompression (7–11 MPa s⁻¹) prior to fragmentation at shallow crustal depths (Fig. 4b, c). The calculated number densities and measured decompression rates are comparable with the VEI 6, 79 AD Vesuvius Plinian eruption (12.8 MPa s⁻¹; Shea et al.

2011), the VEI 5, Towada eruption (0.6–9.1 MPa s⁻¹; Toramaru 2006) and many other end-member silicic eruptions, which have mass discharge rates of around 10⁶–10⁷ kg s⁻¹ (Fig. 5).

Onset of caldera collapse and magma decompression

As inferred from the voluminous lithic clasts in the lag breccia and in line with many other studies, we believe the lag breccias reflect significant vent wall collapse, vent widening and likely caldera collapse. The broad range of pumice clast

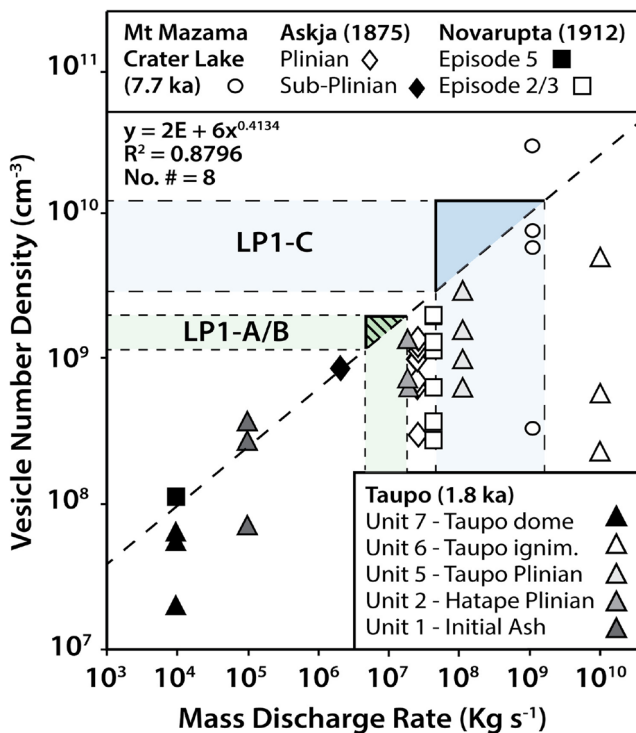


Fig. 5 Vesicle number densities (N_{VF}) for the pre- (LP1-A, B) and syn- (LP1-C) caldera collapse magmas. Included is vesicle number density for other silicic, high intensity and caldera-forming eruptions with inferred MDR assuming a single vent (Young 1990; Klug et al. 2002; Adams et al. 2006; Carey et al. 2010; Houghton et al. 2010). Note. Vesicle number data for the 7.7 ka Crater Lake eruption has a minimum vesicle cutoff of 1 μm . All other data has a minimum vesicle cutoff of 4 μm (Askja, Novarupta and Taupo eruptions). The *oblique dashed line* denotes a line of best fit for pumice with the largest vesicle number density for a specified mass discharge rate (MDR). This plot is used qualitatively to enable comparisons with other data. It is not a definitive assessment of MDR (see Rust and Cashman 2011; Alfano et al. 2012)

densities together with high but variable number densities of small round vesicles in pumice from LP1-C suggests that the magma was in a highly variable state of degassing prior to fragmentation at various lithostatic and magmatic pressures. The development of new and wider conduits at the climax of caldera collapse, as evidenced by the diversity of lithic assemblages, resulted in a two to threefold increase in decompression rate ($15\text{--}28 \text{ MPa s}^{-1}$), a deepening of the fragmentation surface and the incorporation of deep crustal assemblages into the collapsing eruption column (Fig. 4d, e). These results are comparable to other sector (e.g. 1980 Mt. St. Helens eruptions; Toramaru 2006) and lava dome (e.g. 2008 Chaitén eruption; Alfano et al. 2012) collapse events, whereby rapid decompression leads to late-stage explosive magma vesiculation and a deepening of the fragmentation surface. The latter also occurred during other caldera-forming eruptions, including the 172 ka Lower Pumice 2 and 3.6 ka Minoan eruptions (Santorini, Greece; Druitt 2014), the 366 ka Villa Senni eruption (Colli Albani, Italy; Vinkler et al. 2012), the

188 ka Abrigo Ignimbrite eruption (Tenerife, Spain; Pittari et al. 2008), the 36 ka Campanian Ignimbrite eruption (Phlegraean Fields, Italy; Rosi et al. 1996) and the 7.7 ka Crater Lake eruption (Mt. Mazama, USA; Suzuki-Kamata et al. 1993; Fig. 6). Pumice deposited during the caldera-forming Crater Lake eruption also preserve evidence for high magma decompression rates (high vesicle number densities— 10^{10} cm^{-3}) relative to the preceding Plinian eruption phase (10^9 cm^{-3} ; Klug et al. 2002). Together, these data support numerical simulations which predict a $\sim 25 \text{ MPa}$ scale pressure drop at the onset of an idealised caldera collapse event, followed by the downward propagation of the exsolution and fragmentation surfaces by up to 1 km, leading to rapid increases in decompression and mass discharge rates (Folch and Martí 2009).

Geometry and mechanics of caldera collapse driving high magma decompression rates

The deposits of caldera-forming eruptions reflect the style and nature of caldera collapse. Caldera collapse during the Lower Pumice 1 eruption, and other examples of small to moderate Plinian eruptions previously cited, resulted from the breakup of the reservoir roof block and the explosive excavation of large volumes of conduit wall rocks, including deep crustal and hydrothermally altered lithic assemblages, producing voluminous lithic lag breccias. This scenario contrasts with very large caldera systems and their deposits that lack fall deposits and lithic-rich lag breccias, which indicate tectonic opening and passive subsidence of the reservoir roof block along outward-dipping fractures (e.g. 400–600 m thick Toba tuff (71 ka); Rose and Chesner 1987; 100–300 m thick Flemming Hall Ignimbrite; Beddoe-Stephens and Millward 2000; $\sim 300 \text{ m}$ thick Cerro Galan Ignimbrite (2.1 Ma); Cas et al. 2011; Folkes et al. 2011; Gregg et al. 2012). Such a geometry would lead to extensional opening of the vent as the roof block sinks, causing minimal country rock excavation (Acocella 2007; Cas et al. 2011). The occurrence of lithic breccias in the deposits of caldera-forming eruptions may therefore be indicative of vertical or steeply inwards dipping fractures that initially hinder roof block collapse (Gudmundsson 1998). Once these fractures propagate to the Earth's surface, decompression of the magma system to atmospheric pressures induces rapid disequilibrium degassing and the explosive widening of fractures as vents, so allowing roof block collapse (Fig. 4d, e). According to numerical simulations for an ideal 'piston-type' caldera collapse event, the magma reservoir should then repressurise as the roof block subsides, leading to slower, but more predictable, rates of magma decompression (Folch and Martí 2009). However, as evidenced by the diversity of deposits, caldera collapse is rarely simple or uniform. The presence of lag breccias, in particular, would tend to suggest non-ideal 'chaotic' or

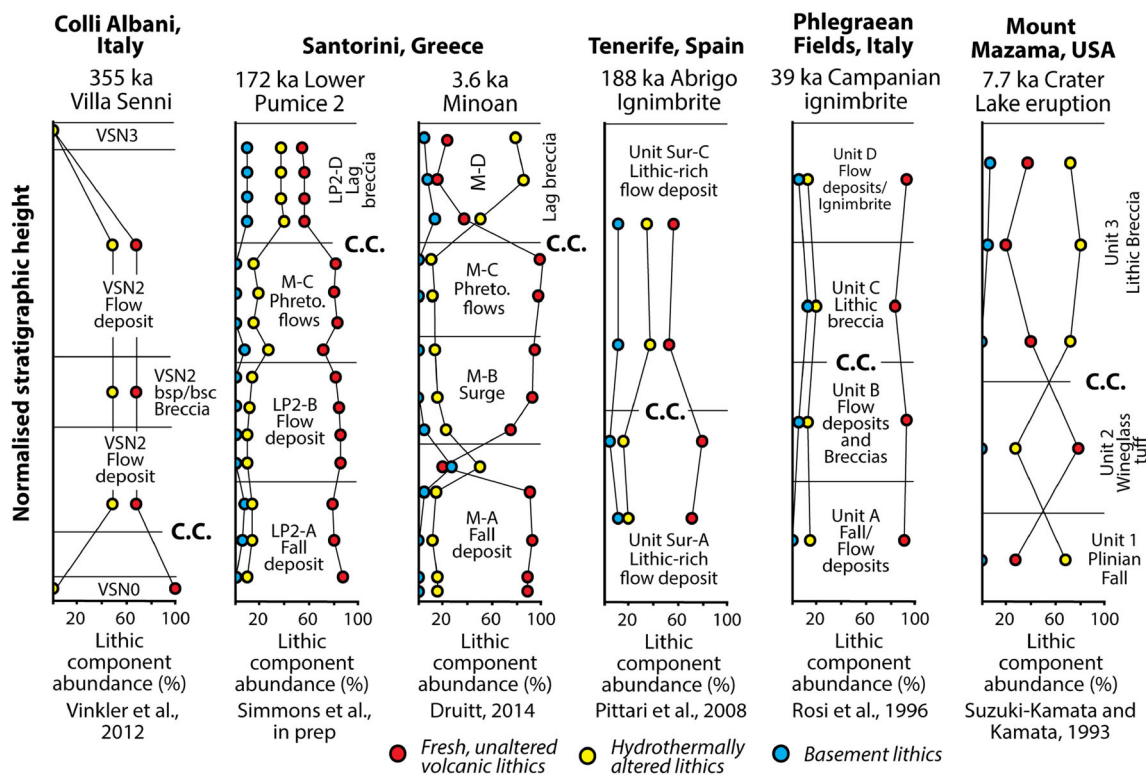


Fig. 6 Variations in lithic components (fresh, altered and basement-derived) within the stratigraphy of other caldera-forming Plinian explosive eruptions that deposited lithic-rich lag breccias. *C.C.* caldera collapse. Note the increase in basement and hydrothermally altered lithic

clasts within the stratigraphy of each eruption sequence, related to caldera collapse and a deepening of the fragmentation surface (Suzuki-Kamata et al. 1993; Rosi et al. 1996; Pittari et al. 2008; Vinkler et al. 2012; Druitt 2014)

‘piecemeal’ caldera collapse. These styles of roof block collapse modify the geometry of the conduit and vent, and in turn the pressure conditions in magma reservoir. For example, the rate of magma decompression decreased by a factor of four during the 1.8 ka caldera-forming eruption of Ksudach Volcano. This was attributed to the development of a conduit with a broad base and a constricted top (Andrews and Gardner 2010). The pressure conditions that result from caldera collapse in the reservoir, conduit and vent, and the associated change in eruption dynamics, are therefore dependent not only on the properties of magma but also on the style of roof block collapse.

Conclusions

This study demonstrates:

- A two to threefold increase in magma decompression rate, corresponding with the development of fractures during the LP1 caldera collapse event, resulted in late-stage explosive magma vesiculation and a deepening of the fragmentation surface.
- Modification of the conduit and vent during catastrophic caldera collapse can alter the pressure conditions in the

magma reservoir and dramatically change the dynamics and intensity of an eruption.

- The occurrence of lithic lag breccias within a deposit sequence can provide important insights into the orientation of fractures, the way they open and widen, and the style of caldera collapse.

Acknowledgments The research was supported by discretionary research funds of R.A.F Cas. This is Laboratory of Excellence ClerVolc contribution number 247. This paper has benefited from constructive reviews by Colin Wilson, Thomas Shea, Joan Marti, Jim Cole, Alain Burgisser and Thomas Giachetti, whom we thank for their suggestions.

References

- Acocella V (2007) Understanding caldera structure and development: an overview of analogue models compared to natural calderas. *Earth-Sci Rev* 85(3–4):125–160
- Acocella V, Cifelli F, Funicello R (2000) Analogue models of collapse calderas and resurgent domes. *J Volcanol Geotherm Res* 104(1–4): 81–96
- Adams NK, Houghton BF, Hildreth W (2006) Abrupt transitions during sustained explosive eruptions: examples from the 1912 eruption of Novarupta, Alaska. *Bull Volcanol* 69(2):189–206
- Alfano F, Bonadonna C, Gurioli L (2012) Insights into eruption dynamics from textural analysis: the case of the May, 2008, Chaitén eruption. *Bull Volcanol* 74(9):2095–2108

- Allen SR, Cas RAF (1998) Lateral variations within coarse co-ignimbrite lithic breccias of the Kos Plateau Tuff, Greece. *Bull Volcanol* 59(5): 356–377
- Andrews BJ, Gardner JE (2010) Effects of caldera collapse on magma decompression rate: an example from the 1800 14C yr BP eruption of Ksudach Volcano, Kamchatka, Russia. *J Volcanol Geotherm Res* 198(1–2):205–216
- Andriessen PAM, Boelrijk NAIM, Hebeda EH, Priem HNA, Verdurnen EAT, Verschure RH (1979) Dating the events of metamorphism and granitic magmatism in the Alpine orogen of Naxos (Cyclades, Greece). *Contr Mineral and Petrol* 69(3):215–225
- Bagdassarov N, Dorfman A, Dingwell DB (2000) Effect of alkalis, phosphorus, and water on the surface tension of haplogranite melt. *Am Mineral* 85(1):33–40
- Bailey RA (1994) Physical geology and eruptive history of the Matahina Ignimbrite, Taupo Volcanic Zone, North Island, New Zealand. *NZ J Geol Geophys* 37(3):319–344
- Bear AN, Cas RAF, Giordano G (2009) Variations in eruptive style and depositional processes associated with explosive, phonolitic composition, caldera-forming eruptions: the 151 ka Sutri eruption, Vico Caldera, central Italy. *J Volcanol Geotherm Res* 184(3–4):225–255
- Beddoe-Stephens B, Millward D (2000) Very densely welded, rheomorphic ignimbrites of homogeneous intermediate calc-alkaline composition from the English Lake District. *Geol Mag* 137(2):155–173
- Behrens H, Zhang Y, Xu Z (2004) H₂O diffusion in dacitic and andesitic melts. *Geochim Cosmochim Acta* 68(24):5139–5150
- Brown RJ, Orsi G, De Vita S (2008) New insights into Late Pleistocene explosive volcanic activity and caldera formation on Ischia (southern Italy). *Bull Volcanol* 70(5):583–603
- Cadoux A, Scaillet B, Druitt TH, Deloule E (2014) Magma storage conditions of large Plinian eruptions of Santorini Volcano (Greece). *J Petrol* 55(6):1129–1171
- Carey RJ, Houghton BF, Thordarson T (2010) Tephra dispersal and eruption dynamics of wet and dry phases of the 1875 eruption of Askja Volcano, Iceland. *Bull Volcanol* 72(3):259–278
- Cas RAF, Wright HMN, Folkes CB, Lesti C, Porreca M, Giordano G, Viramonte JG (2011) The flow dynamics of an extremely large volume pyroclastic flow, the 2.08-Ma Cerro Galán Ignimbrite, NW Argentina, and comparison with other flow types. *Bull Volcanol* 73(10):1583–1609
- Druitt TH (1985) Vent evolution and lag breccia formation during the Cape Riva eruption of Santorini, Greece. *J Geol* 93(4):439–454
- Druitt TH (2014) New insights into the initiation and venting of the Bronze-Age eruption of Santorini (Greece), from component analysis. *Bull Volcanol* 76(2):1–21
- Druitt TH, Bacon CR (1986) Lithic breccia and ignimbrite erupted during the collapse of Crater Lake Caldera, Oregon. *J Volcanol Geotherm Res* 29(1–4):1–32
- Druitt TH, Edwards L, Mellors RM, Pyle DM, Sparks RSJ, Lanphere M, Davies M, Barreiro B (1999) Santorini Volcano. The Geological Society, London
- Druitt TH, Francaviglia V (1992) Caldera formation on Santorini and the physiography of the islands in the late Bronze Age. *Bull Volcanol* 54(6):484–493
- Folch A, Martí J (2009) Time-dependent chamber and vent conditions during explosive caldera-forming eruptions. *Earth Planet Sci Lett* 280(1–4):246–253
- Folkes C, Wright H, Cas RF, de Silva S, Lesti C, Viramonte J (2011) A reappraisal of the stratigraphy and volcanology of the Cerro Galán volcanic system, NW Argentina. *Bull Volcanol* 73(10):1427–1454
- Gardner JE, Hilton M, Carroll MR (1999) Experimental constraints on degassing of magma: isothermal bubble growth during continuous decompression from high pressure. *Earth Planet Sci Lett* 168(1–2): 201–218
- Gardner JE, Ketcham RA, Moore G (2013) Surface tension of hydrous silicate melts: constraints on the impact of melt composition. *J Volcanol Geotherm Res* 267:68–74
- Gertisser R, Preece K, Keller J (2009) The Plinian Lower Pumice 2 eruption, Santorini, Greece: magma evolution and volatile behaviour. *J Volcanol Geotherm Res* 186(3–4):387–406
- Gregg PM, de Silva SL, Grosfils EB, Parmigiani JP (2012) Catastrophic caldera-forming eruptions: thermomechanics and implications for eruption triggering and maximum caldera dimensions on Earth. *J Volcanol Geotherm Res* 241–242:1–12
- Gudmundsson A (1998) Formation and development of normal-fault calderas and the initiation of large explosive eruptions. *Bull Volcanol* 60(3):160–170
- Hasegawa T, Matsumoto A, Nakagawa M (2016) Evolution of the 120 ka caldera-forming eruption of Kutcharo volcano, eastern Hokkaido, Japan: geologic and petrologic evidence for multiple vent systems and rapid generation of pyroclastic flow. *J Volcanol Geotherm Res* 321:58–72
- Houghton BF, Carey RJ, Cashman KV, Wilson CJN, Hobden BJ, Hammer JE (2010) Diverse patterns of ascent, degassing, and eruption of rhyolite magma during the 1.8ka Taupo eruption, New Zealand: evidence from clast vesicularity. *J Volcanol Geotherm Res* 195(1):31–47
- Jackson J (1994) Active tectonics of the Aegean region. *Annu Rev Earth Planet Sci* 22(1):239–271
- Keller J, Kraml M, Schwarz M (2000) Dating major volcanic paroxysms within the deep-sea record: the example of the Thera Formation, Santorini, Greece. In: IAVCEI General Assembly. Bali, Indonesia, p 16
- Klug C, Cashman K, Bacon C (2002) Structure and physical characteristics of pumice from the climactic eruption of Mount Mazama (Crater Lake), Oregon. *Bull Volcanol* 64(7):486–501
- Mastin LG (2001) A simple calculator of ballistic trajectories for blocks ejected during volcanic eruptions. In: US Geological Survey, p 16
- Milner DM, Cole JW, Wood CP (2003) Mamaku Ignimbrite: a caldera-forming ignimbrite erupted from a compositionally zoned magma chamber in Taupo Volcanic Zone, New Zealand. *J Volcanol Geotherm Res* 122(3–4):243–264
- Mourtada-Bonnefoi CC, Laporte D (2002) Homogeneous bubble nucleation in rhyolitic magmas: an experimental study of the effect of H₂O and CO₂. *Journal of Geophysical Research: Solid Earth* 107(B4):ECV 2–1–ECV 2–19
- Nairn IA, Wood CP, Bailey RA (1994) The Reporoa caldera, Taupo Volcanic Zone: source of the Kaingaroa Ignimbrites. *Bull Volcanol* 56(6–7):529–537
- Nicholls IA (1971) Petrology of Santorini Volcano, Cyclades, Greece. *J Petrol* 12(1):67–119
- Palladino DM, Simeï S (2005) Eruptive dynamics and caldera collapse during the Onano eruption, Vulcini, Italy. *Bull Volcanol* 67(5):423–440
- Papanikolaou DJ (1987) Tectonic evolution of the Cycladic blueschist belt (Aegean Sea, Greece). In: Helgeson H (ed) chemical transport in metasomatic processes. Springer Netherlands, pp 429–450
- Pensa A, Cas R, Giordano G, Porreca M, Wallenstein N (2015) Transition from steady to unsteady Plinian eruption column: the VEI 5, 4.6 ka Fogo A Plinian eruption, São Miguel, Azores. *J Volcanol Geotherm Res* 305:1–18
- Pittari A, Cas RAF, Wolff JA, Nichols HJ, Larson PB, Martí J (2008) Chapter 3 The use of lithic clast distributions in pyroclastic deposits to understand pre- and syn-caldera collapse processes: a case study of the Abrigo ignimbrite, Tenerife, Canary Islands. In: Joachim G, Joan M, iacuta (eds) developments in volcanology. Elsevier, pp 97–142
- Reubi O, Nicholls IA (2004) Variability in eruptive dynamics associated with caldera collapse: an example from two successive eruptions at Batur volcanic field, Bali, Indonesia. *Bull Volcanol* 66(2):134–148

- Rose WI, Chesner CA (1987) Dispersal of ash in the great Toba eruption, 75 ka. *Geology* 15(10):913–917
- Rosi M, Vezzoli L, Aleotti P, De Censi M (1996) Interaction between caldera collapse and eruptive dynamics during the Campanian Ignimbrite eruption, Phlegraean Fields, Italy. *Bull Volcanol* 57(7): 541–554
- Rotella MD, Wilson CJN, Barker SJ, Cashman KV, Houghton BF, Wright IC (2014) Bubble development in explosive silicic eruptions: insights from pyroclast vesicularity textures from Raoul volcano (Kermadec arc). *Bull Volcanol* 76(8):826
- Rust AC, Cashman KV (2011) Permeability controls on expansion and size distributions of pyroclasts. *J Geophys Res B: Solid Earth* 116(11)
- Sahagian DL, Proussevitch AA (1998) 3D particle size distributions from 2D observations: stereology for natural applications. *J Volcanol Geotherm Res* 84(3–4):173–196
- Schliestedt M, Altherr R, Mathews A (1987) Evolution of the Cycladic crystalline complex: petrology, isotope geochemistry and geochronology. In: Helgeson R (ed) *Chemical processes in metasomatic processes*. Reidal, Dordrecht, pp 389–428
- Shea T, Gurioli L, Houghton BF, Cioni R, Cashman KV (2011) Column collapse and generation of pyroclastic density currents during the A.D. 79 eruption of Vesuvius: the role of pyroclast density. *Geology* 39(7):695–698
- Shea T, Houghton BF, Gurioli L, Cashman KV, Hammer JE, Hobden BJ (2010) Textural studies of vesicles in volcanic rocks: an integrated methodology. *J Volcanol Geotherm Res* 190(3–4):271–289
- Silva C (2008) Reconstruction and eruptive dynamics of the Holocene basaltic-andesitic Pucón Ignimbrite. University of Blaise Pascal, University of Blaise Pascal, In
- Simmons JM, Cas RAF, Druitt TH, Folkes CB (2016) Complex variations during a caldera-forming Plinian eruption, including precursor deposits, thick pumice fallout, co-ignimbrite breccias and climactic lag breccias: the 184 ka Lower Pumice 1 eruption sequence, Santorini, Greece. *J Volcanol Geotherm Res* 324:200–219
- Suzuki-Kamata K, Kamata H, Bacon CR (1993) Evolution of the caldera-forming eruption at Crater Lake, Oregon, indicated by component analysis of lithic fragments. *J Geophys Res* 98(B8):14059–14074
- Toramaru A (2006) BND (bubble number density) decompression rate meter for explosive volcanic eruptions. *J Volcanol Geotherm Res* 154(3–4):303–316
- Vespa M, Keller J, Gertisser R (2006) Interplinian explosive activity of Santorini volcano (Greece) during the past 150,000 years. *J Volcanol Geotherm Res* 153(3–4):262–286
- Vinkler AP, Cashman KV, Giordano G, Groppelli G (2012) Evolution of the mafic Villa Senni caldera-forming eruption at Colli Albani volcano, Italy, indicated by textural analysis of juvenile fragments. *J Volcanol Geotherm Res* 235–236:37–54
- Walker GPL (1985) Origin of coarse lithic breccias near ignimbrite source vents. *J Volcanol Geotherm Res* 25(1–2):157–171
- Wilson CJN (2001) The 26.5 ka Oruanui eruption, New Zealand: an introduction and overview. *J Volcanol Geotherm Res* 112(1–4): 133–174
- Young SR (1990) Physical volcanology of Holocene airfall deposits from Mt. Mazama, Crater Lake, Oregon. In: University of Lancaster,
- Zhang Y, Behrens H (2000) H₂O diffusion in rhyolitic melts and glasses. *Chem Geol* 169(1–2):243–262